Materials and Structures (2013) 46:2013–2028
DOI 10.1617/s11527-013-0033-5

ORIGINAL ARTICLE

Rotation capacity and stress redistribution ability of R-UHPFRC–RC composite continuous beams: an experimental investigation

Talayeh Noshiravani · Eugen Brühwiler

Received: 20 March 2012 / Accepted: 14 February 2013 / Published online: 21 February 2013

Abstract The results of tests on two continuous composite beams combining a reinforced concrete (RC) beam with a layer of reinforced ultra-high performance fiber reinforced concrete (R-UHPFRC) are presented. The R-UHPFRC element acts both as a tensile membrane and a flexural element. The tests show the element's contribution to the member capacity by allowing the redistribution of the internal forces. The continuous beams are placed on two intermediate supports; the shear span-depth ratios and stirrup content are chosen to provoke two successive formations of local flexure-shear collapse mechanisms, forming a plastic hinge at each support. With the formation of the first support hinge, the stresses redistribute. As the applied actuator displacement increases, the member continues to resist the increasing force up to the formation of a second support hinge that causes the member to collapse. The member deflection and resistance at collapse were respectively 4.5 and 1.3 times greater than the corresponding values at the formation of the first hinge. The response demonstrates the redundancy in RC beams with additional R-UHPFRC reinforcement, which can be used for designing structures against progressive collapse.

Keywords UHPFRC · Composite beam · Shear · Hinge · Stress redistribution · Redundancy · Post-peak resistance

List of symbols

Mathematical symbols and axes

x,z	Longitudinal and vertical axis from a chosen origin (i.e., bottom concrete fiber at midspan for the continuous beam specimens and at the roller support for the cantilever beam specimen); or a component of a dimension or vector along the axes
Δ	Difference (e.g., ΔT)
Σ	Sum

Subscripts

0 or 1	For the continuous beam tests, the subscripts 0 or 1 are related to the location of the imposed displacement at the cantilever ends or at the jack at mid span
1 or 2	In the Flexure–Shear collapse mechanism, the subscripts 1 or 2 refer to the two R-UHPFRC hinges at the extremities of the ICD zone
R	Resistance (e.g., M_R)

T. Noshiravani (✉)
Zilch+Müller Ingenieure, Munich, Germany
e-mail: talayeh.noshiravani@epfl.ch;
talayeh.noshiravani@a3.epfl.ch

T. Noshiravani · E. Brühwiler
École Polytechnique Fédérale de Lausanne (EPFL),
Lausanne, Switzerland
e-mail: eugen.bruehwiler@epfl.ch
URL: http://mcs.epfl.ch/page-7840.html

FS	Related to the Flexure–Shear crack or collapse mechanism
ICD	ICD zone
U	UHPFRC material or of an R-UHPFRC section or hinge
c	Concrete
i	Steel or UHPFRC reinforcement
max	Maximum
mid	Related or with respect to midspan
p	Related or with respect to the pin support
r	Related or with respect to roller support; except in f_{Ur}
sU	Rebars in the R-UHPFRC element
st	Tensile rebars in the RC element
sv	Steel stirrups
u	Maximum or ultimate resistance; strength; resistance at peak
v	Related to vertical shear reinforcement

Roman (upper case)

A	Area
A_{sv}	Stirrup area within the stirrup spacing s
E_c	Young's modulus of elasticity of concrete
E_s	Young's modulus of elasticity of steel
E_U	Young's modulus of elasticity of UHPFRC
$E_{U,H}$	Stiffness of UHPFRC in the strain hardening phase
M	Moment
Q	Forces acting on the continuous beam specimens
R	Reaction force
T	Tension force
V	Shear force or the force action on a cantilever beam specimen
$V_{c,CSCT}$	Shear resistance based on the Critical Shear Crack Theory

Roman (lower case)

a	Shear span
a/d	Shear span-depth ratio
b	Beam width
c	Height of the neutral axis from the extreme concrete compressive fiber
d	Effective depth (when without a subscript)
d_i	Depth of reinforcement i with respect to the extreme compressive concrete fiber
f_i	Elastic limit strength of reinforcement i (i.e. f_{sy} or $f_{Ut,el}$)
f_c	Concrete cylinder compressive strength
$f_{c,cube}$	Concrete cube compressive strength
f_{ct}	Concrete tensile strength
f_{sy}	Steel yield stress
f_{su}	Steel tensile strength
f_{Uc}	UHPFRC average compressive strength
f_{Ur}	UHPFRC modulus of rupture
$f_{Ut,el}$	UHPFRC elastic tensile strength
$f_{Ut,u}$	UHPFRC maximum tensile strength
$f_{Ut,S}$	UHPFRC tensile-softening resistance
h	Height
l	Length
s	Stirrup spacing
w	Crack width

Greek

ε_{sy}	Steel strain at the yield stress
ε_{su}	Steel strain at the ultimate strength
$\varepsilon_{Ut,u}$	UHPFRC tensile strain at the maximum tensile strength
ρ_v	Ratio of transverse reinforcement in the RC element
ω_i	Mechanical reinforcement ratio of reinforcement i
ψ	Rotation of a beam or an R-UHPFRC hinge (i.e., ψ_U)
θ_c	Measured angle of the collapse crack in concrete
Δ	Beam displacement with respect to the strong floor

1 Introduction

An emerging strengthening technique for continuous reinforced concrete (RC) floor slabs and bridge decks is the addition of a thin layer of ultra-high performance fiber reinforced concrete (UHPFRC) reinforced with small-diameter steel rebars [2]. In tension, the reinforced UHPFRC (R-UHPFRC) layer primarily acts as an added flexural reinforcement for the RC element. Applicable to both existing and new structures, this method modifies an RC member into a composite R-UHPFRC–RC (RU–RC) member (Fig. 1a) with a higher performance in terms of resistance, deformation capacity and durability.

UHPFRC belongs to the family of high performance fiber reinforced cementitious composites [14]. The material has a compact, quasi-impermeable matrix, high strength and deformation capacity in tension. UHPFRC is distinguished as a material exhibiting

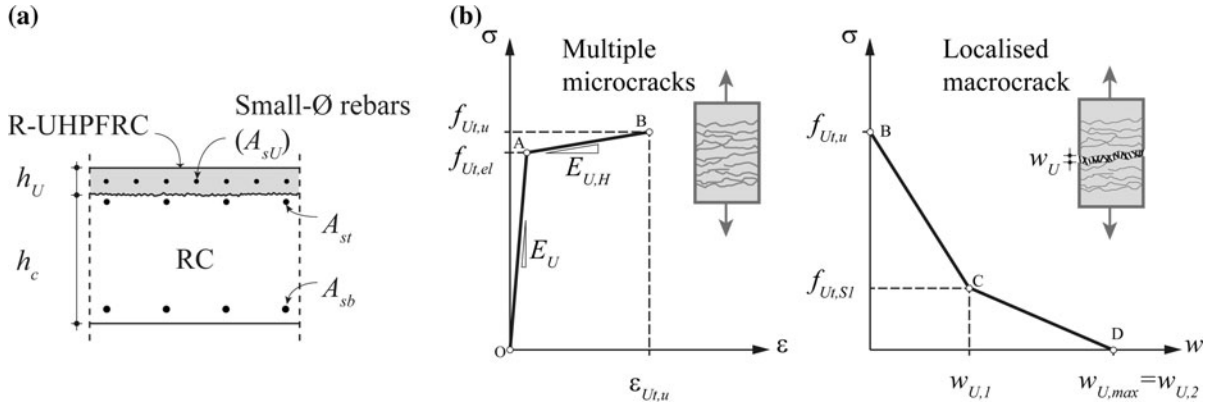

Fig. 1 **a** Cross section of an RU–RC slab strip; **b** Constitutive laws of UHPFRC [17]

strain hardening in tension [20]. Figure 1b illustrates the tensile behavior of UHPFRC in three phases. In the first phase, the material is elastic with a similar modulus of elasticity as that of concrete. In the second phase, the material goes into strain hardening with multiple microcracking of the matrix and fiber activation. In the third phase, a discrete macro crack begins to develop. Along this crack, fiber pullout and material strain softening occur. The nonlinear tensile behavior of UHPFRC depends on the random orientation and distribution of the discontinuous fibers [18, 22]. To prevent fiber orientation and distribution to hinder the properties of UHPFRC, the layer has to be reinforced with steel rebars.

The properties of strain-hardening UHPFRC make it possible to use relatively thin layer of R-UHPFRC on RC elements as both an additional flexural reinforcement and a protective layer. For slab like elements, Habel et al. (2006) recommend an R-UHPFRC layer thickness between 30 and 80 mm (1.81 and 3.15 in).

In RU–RC slabs or beams (Fig. 1a), the R-UHPFRC layer can be either cast in place or glued as prefabricated elements to the surface of an RC member [1, 6]. Casting is done over a rough surface of concrete where the bond is provided by the chemical adherence of the new cement to the old concrete surface and the roughness of the interface. Dowels or stirrups are not required to connect the two layers. Researchers have independently shown that debonding only begin after the strain-hardening phase and as the steel rebars begin to yield [1, 5].

The monolithic action between concrete and UHPFRC is due to their compatible material properties and the controlled crack opening in the RC element. It is the combination of the mechanical properties of UHPFRC, namely its similar modulus of elasticity to concrete, its high tensile strength and its strain hardening behavior that allows the layer to deform together with the RC element. Meanwhile, together the strain hardening UHPFRC and the steel reinforcement resist the opening of flexural cracks in the RC element and hinder the concrete fracture due to in-plane shear that would otherwise cause the debonding between the two elements [5, 21]. The small-diameter steel reinforcing bars improve the strain hardening behavior of R-UHPFRC, thus contributing to the monolithic action with the RC element [18].

Flexural strengthening of RC elements is often limited by their shear carrying capacity. Similar to RC beams, the opening and full development of a flexural-shear crack in the RC element of an RU–RC beam leads to the local flexure-shear collapse of the composite member [1, 16]. When subjected to high shear forces, RU–RC members are susceptible to intermediate-crack-induced debonding (ICD) that softens the connection between the two elements [17]. Thus, the RU–RC members change from a monolithic member to a two-layer member with an interlayer slip. As illustrated in Fig. 2, the relative vertical movement of the RC segments separated by an inclined flexure-shear crack generates prying stresses on the R-UHPFRC layer. These stresses are resisted by the R-UHPFRC tensile element bending in double curvature.

Recently, Noshiravani and Brühwiler [17] showed that R-UHPFRC layers not only increase the flexural strength but also the shear resistance and the deformation capacity of RC beams subjected to combined

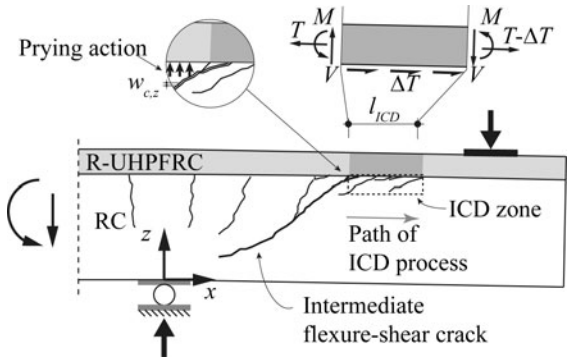

Fig. 2 Intermediate-crack-induced debonding in RU–RC elements [17]

bending and shear. The contribution of the tensile R-UHPFRC element to the shear resistance is twofold. First, the element resists the out-of-plane prying stresses by bending in double curvature (Fig. 1b). Second, by acting as an external tensile reinforcement, the element controls the width of cracks in concrete, thus increasing the concrete contribution to the shear resistance. Both mechanisms are inversely related to the length of the ICD zone between the RC and R-UHPFRC elements [16]. While the former mechanism continues to contribute to the shear resistance of the layer after a flexure-shear failure, the latter is replaced by the tensile membrane action of the R-UHPFRC reinforcement layer, similar as that in RC members [10].

Following the maximum flexural-shear resistance of RU–RC beams (peak), the R-UHPFRC element continues to contribute to the shear resistance of the member (in the post-peak regime) [16]. The high residual resistance of the elements in the post-peak regime is redundant for the case of a statically determinate system. Nevertheless, it is relevant in the case of an indeterminate system that allows load redistribution following a local failure in order to avoid a progressive collapse. This paper presents an experimental investigation on continuous RU–RC beams that demonstrate the contribution of the R-UHPFRC layer to the member robustness.

2 Significance of research

In recent years, the application of R-UHPFRC layers for strengthening of more than 15 continuous bridge decks and floor slabs in Switzerland has demonstrated the potential of this novel intervention method. It has been shown that when subject to high shear stresses, R-UHPFRC reinforcement increases both member shear resistance and deformation capacity [17]. There is experimental evidence that the R-UHPFRC layer significantly increases the residual resistance following the formation of a support hinge or the punching of an RC beam or slab, respectively [16, 22]. This residual resistance is especially useful for design of redundant continuous structures to prevent their progressive collapse following a local failure. Can an R-UHPFRC layer help to carry the redistributed stresses in continuous beams and one-way slabs in the event of a local flexural-shear failure? How does the stress redistribution change the global behavior of continuous members? This research aims to provide a better understanding of the inherent redundancy in RU–RC flexural members.

3 Background

3.1 Shear resistance of RU–RC beams

Similar to RC beams [7, 11], the shear resistance of RU–RC beams and one-way slabs depends on the following four parameters:

The first parameter is the shear span-depth ratio (a/d), where the effective depth (d) is defined as

$$d = \Sigma(d_i \cdot A_i \cdot f_i \cdot)/\Sigma(A_i \cdot f_i) \quad (1)$$

In Eq. (1), i refers to each reinforcement, namely the steel rebars in concrete and UHPFRC and the UHPFRC layer; d_i is the distance between the centerline of each reinforcement to the extreme compressive fiber; A_i is the reinforcement area; and f_i is the elastic limit strength, that is the yield strength of steel or the tensile resistance of UHPFRC at the end of its elastic phase.

The second parameter is the ratio of shear reinforcement (ρ_v) in the RC element:

$$\rho_v = A_{sv}/(s \cdot b) \quad (2)$$

where A_{sv} is the stirrup area; s is the stirrup spacing; and b is the beam width.

The third parameter is the amount of longitudinal reinforcement, expressed as the sum of the mechanical reinforcement ratio of each reinforcement (ω_i):

$$\omega_i = (A_i \cdot f_i)/(A_c \cdot f_c) \quad (3)$$

where A_c and f_c are the concrete area and compressive strength, respectively.

Finally, the fourth parameter is the bond condition of each reinforcement. Here, the bond between the UHPFRC and concrete that is influenced by the ICD zone.

Figure 3 shows the member response and crack pattern of the two beams from a series of tests on cantilever beams [15]. In this figure, the structural response is shown as the plot of the force at the end of the cantilever span (V) versus the beam deflection (Δ) at the jack. The deflection is measured with respect to the strong floor. The beams have $a/d = 3.0$ and the same total mechanical reinforcement ratio $\Sigma\omega_i = 29.9$ %. The stirrups spacing is chosen so that ρ_v in beams MN3 and MW6 are 0.15 and 0.09 %, respectively. Both beams fail in combined flexure and shear. As illustrated in Fig. 3b, at 93 and 97 % of the ultimate force V_u, the maximum measured crack widths of the flexure-shear collapse cracks in the RC are between 1.6 and 2.0 mm. Close to failure, the web deformations in beam MW6 are concentrated at the flexure-shear collapse crack and member rotation is about the tip of this crack. In contrast, the web deformation in the beam MN3 is distributed between two main inclined cracks, crossing the two-legged closed stirrups in the shear span.

The critical shear crack theory (CSCT) [13] for beams with no shear reinforcement is used to evaluate the gain in shear resistance due to stirrups and the R-UHPFRC layer. The CSCT expresses the failure of a beam in terms of its resistance as the function of rotation. The rotation of the beam is due to the opening of a flexural-shear crack at which the deformations localize and a flexural-shear failure eventually occurs. To predict the failure of member with shear reinforcement, the contribution of steel stirrups can be added to the original failure envelope of the CSCT [12].

The response of beam MW6 with a very low ρ_v was compared to the prediction of the CSCT for beams. This comparison is possible because the flexural-shear collapse crack in beam MW6 does not cross a stirrup in the web, except at the crack tip close to the roller support where the stirrup contribution in resisting the crack opening is negligible. The vertical and horizontal offset of the peak with respect to the CSCT failure criterion as a function of member rotation can give insight into the contribution of the R-UHPFRC element to the member response. In the case of beam MW6, the deformation capacity is 75 % higher than that estimated by the CSCT for a similar RC member with an equivalent amount of longitudinal reinforcement [17].

In Fig. 3, the failure envelope for beam MN3 is calculated from the superposition of the CSCT function and the contribution of the steel stirrups with a bi-linear stress–strain relationship. The failure envelope is thus defined by a two-phase function. In the first phase, the stirrups are elastic. As the concrete crack opens, the force carried by the stirrups increases. The function changes when the stirrups begin to yield. In the second phase, the function is defined by the superposition of the constant force carried by the yielding stirrups and the decreasing contribution of

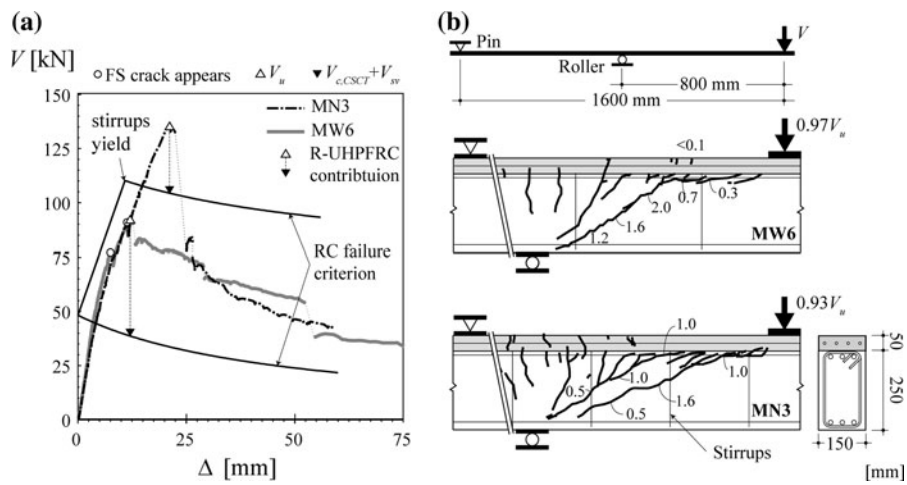

Fig. 3 Results of two RU–RC cantilever beam tests [17]: **a** Shear force–deflection response; **b** Crack pattern before flexure–shear failure

concrete along the critical shear crack, as defined by the CSCT. The failure envelope does not consider the contribution of the R-UHPFRC to the member shear resistance. The plot shows that the shear resistance of beam MN3 is higher than the maximum resistance of the envelope. Furthermore, the failure of the beam occurs after the yielding of the stirrups. The high resistance and deformation capacity of beam MN3 are due to the interaction between its R-UHPFRC and RC elements.

The shear resistance of RU–RC beams is indeed the sum of the contributions of concrete (V_c), of the stirrups (V_s), and of the R-UHPFRC element in double bending (V_U) [16]. The test results of beams MN3 and MW6 show that V_U can be as much as 30 % of the ultimate force acting on the beams [16, 17]. A flexure–shear collapse mechanism (Fig. 4) is formed when the applied force exceeds the sum of the contributions of the two elements. The collapse mechanism occurs with the crushing of concrete in front of the tip of the collapse crack.

3.2 Plastic hinges in RU–RC beams

Plastic hinges define local zones in a member or elements where the deformation localizes and the plastic member rotation occurs. The term has been separately used for reinforced concrete beams [3, 4] and reinforced concretes [8, 9, 19].

For the purpose of RU–RC members, it is necessary to distinguish between the R-UHPFRC element hinges and the RU–RC member hinge. R-UHPFRC hinges form with the ICD as the element is subjected to combined tension and bending. RU–RC hinges can either be monolithic or two-layer including the ICD zone. RU–RC hinges form due to the negative moment

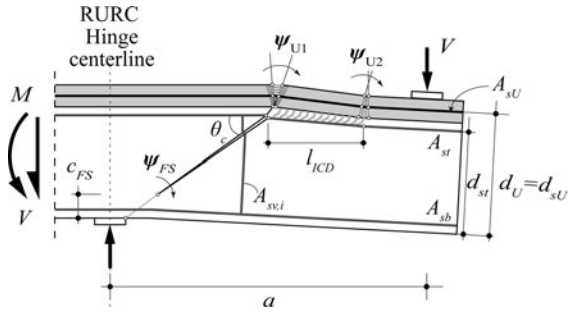

Fig. 4 Development of Flexure-Shear collapse mechanism in RU–RC beams [16]

over intermediate supports. Therefore, in this paper, they are also referred to as support hinges. The force that initiates the plastic rotation of an RU–RC hinge is referred to as the hinging resistance.

The resistance of a support hinge is the combination of the contributions of the R-UHPFRC plastic hinges and of the steel reinforcement in the RC element. The latter is comprised of the dowel and membrane actions of the compressive and tensile longitudinal rebars, respectively, and the force carried by the stirrups. The post-peak curves of the response of the cantilever beams in Fig. 3 illustrate the typical behavior of a support hinge. The force–deflection response of a member following the formation of a support hinge is referred to as the post-hinging response.

The post-hinging response of RU–RC beams is of interest in the design of structures that require structural redundancy and the ability for load redistribution following the formation of a flexure–shear collapse mechanism, thus preventing a progressive collapse.

To investigate the contribution of R-UHPFRC to the rotation capacity and the ability of internal-force redistribution in continuous RU–RC members, a series of tests on RU–RC beams was carried out. This paper presents the experiments and test results of two of the continuous beams. The cantilever beams presented in Fig. 3 are used as the reference beams for the shear reinforcement design in each half of the continuous beams. The tests demonstrate the contribution of the R-UHPFRC element to the RU–RC members' resistance, rotation capacity, and ability to redistribute stress.

4 Experiments

4.1 Test specimens

Figure 5 shows the test setup, static system, geometry, and reinforcement detailing of the two continuous RU–RC beams [15]. The beams represent slab ribs or thin one-way slabs strips.

R-UHPFRC layers are typically added to an existing or a precast concrete element. For the purpose of the experiments, the composite beams are constructed in two casting stages. In the first stage, the RC element is cast. A set retarder is used on the formwork face receiving the concrete surface that is later at the

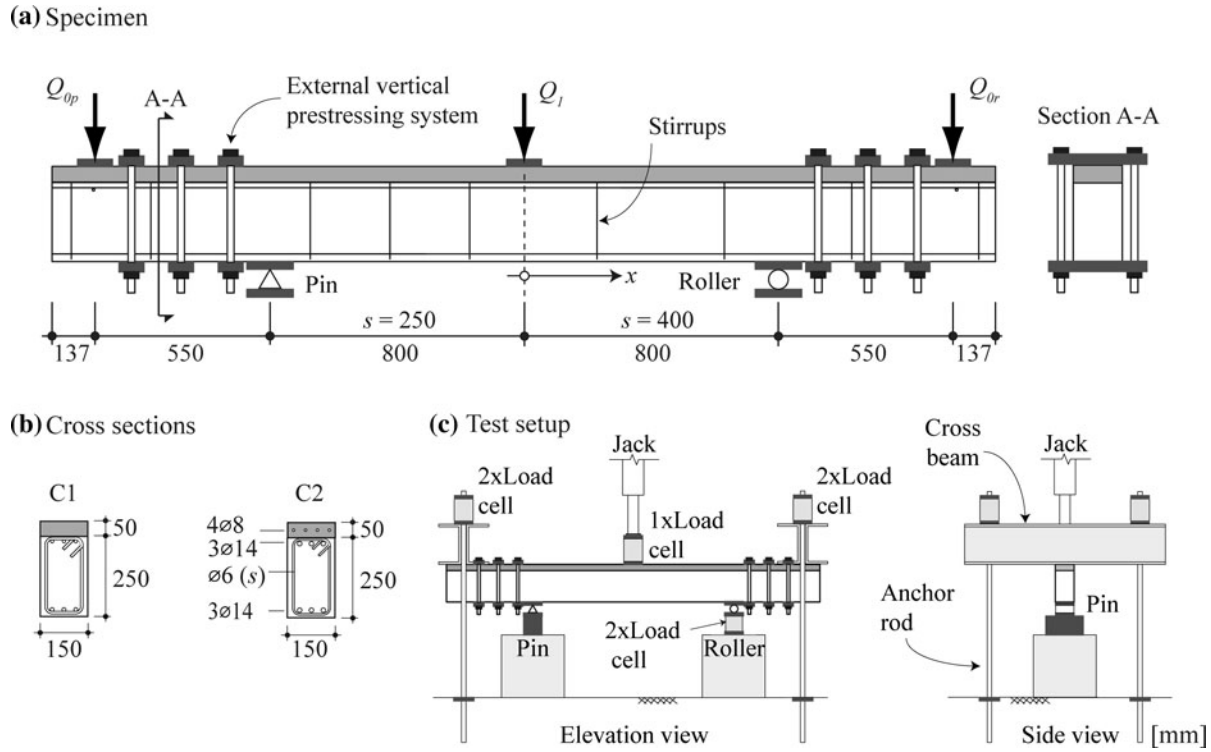

Fig. 5 Specimens and test setup

interface between RC and R-UHPFRC elements. After demoulding, the soft concrete above the rebars is removed using a light hydrodemolition of the concrete cover to expose the aggregates. Following this process, the longitudinal rebars remained below a minimum of 6-mm thick concrete cover (*i.e.*, same as the diameter size of the stirrups). In the second stage, the R-UHPFRC element is cast on the rough concrete surface. The bond between the elements is a combination of the chemical bond between the UHPFRC and concrete as well as the roughness of the concrete surface.

The beams are 150 mm wide and 300 mm high, comprising a 50-mm thick UHPFRC layer and a 250-mm high RC element. The continuous beams have a total length of 2.98 m, divided into a 1.60-m long center span and two 0.69-m long cantilever spans. With a shear span-to-depth ratio (a/d) of 3.0, each half of the central span matches the 0.8-m long cantilever beams in Fig. 3 [15, 17]. In the aforementioned ratio, d is calculated using Eq. (1).

Except for the number and type of rebars in the R-UHPFRC elements, the beams have the same reinforcement detailing. The longitudinal rebars are anchored with welded cross bars outside the main spans. The RC elements are reinforced with two-legged closed stirrups having a diameter of 6 mm. At the mid span, s varies from 250 to 400 mm; thus, ρ_v changes from 0.15 to 0.09 %, matching the shear reinforcement in beam MN3 and MW6, respectively [17]. The different reinforcement is chosen to provoke an early formation of a flexure-shear collapse mechanism in the intermediate span close to the roller support.

Table 1 summarizes the test parameters for each beam. For ρ_v and s, the subscripts p or r (for pin or roller) are used to denote the difference between the shear reinforcement in each half of the intermediate span. The three types of longitudinal reinforcement are distinguished with the subscripts: st (RC rebars), U (UHPFRC section) and sU (R-UHPFRC rebars).

4.2 Material properties

The tests presented herein were a part of a larger test program [15] for which all beams were cast at the same

Table 1 Continuous beams and their reference cantilever beams

Beam	s_p^a (mm)	s_r^b (mm)	$\rho_{v,p}^a$ (%)	$\rho_{v,r}^b$ (%)	ω_{st} (%)	ω_U (%)	ω_{sU} (%)
Cantilever beams							
MW6	–	400	–	0.09	16.8	3.9	9.2
MN3	–	250	–	0.15	16.8	3.9	9.2
Continuous beams							
C1	250	400	0.15	0.09	16.8	3.9	0
C2	250	400	0.15	0.09	16.8	3.9	7.3

Note Spacing (s) and ratio (ρ_v) of RC transversal reinforcement in the spans between

[a] The jack and the pin

[b] The jack and the roller

Table 2 Tested material properties [18]

Concrete						
E_c (GPa)		$f_{c,cube}$ (MPa)		f_c (MPa)		f_{ct} (MPa)
31.6		49.2		41.5		4.23
UHPFRC						
Elastic		Strain hardening		Strain softening		
E_U (GPa)	$f_{Ut,el}$ (MPa)	$\varepsilon_{Ut,u}$ (%)	$f_{Ut,u}$ (MPa)	w_U (mm)	$f_{Ut,S}$ (MPa)	
48.0	10.2	0.1–0.4	12.5	3	4	
				6.5	0	
Steel						
ϕ (mm)	E_s (GPa)	f_{sy} (MPa)	ε_{su} (%)	f_{su} (MPa)	f_{su}/f_{sy}	Surface
6	210	626	3.70	655	1.05	Ribbed
8		710	2.20	906	1.27	Ribbed
14		565*	9.79	663	1.17	Ribbed

* The yield plateau end at an average strain of 2 %

time. The continuous beams were tested between 414 and 435 days after casting. The material properties are given in Table 2.

Conventional ready mixed concrete with an aggregate size of 16 mm was used to cast the RC elements in both beam series. Table 2 provides the average values of the material properties based on the standardized tests. The properties of concrete are from tests at the age of 441 days.

The strain-hardening UHPFRC mix was developed by Oesterlee [18]. The average UHPFRC cylinder compressive strength (f_{Uc}) and Modulus of Rupture (f_{Ur}) at the age of 412 days were 228 and 52.9 MPa, respectively. The UHPFRC tensile properties tested by Oesterlee (2010) are also listed in Table 2. These properties are achieved through a mix design that include a 3 % volume of straight steel fibers; quartz sand with a maximum aggregate size of 0.5 mm as the only aggregate; high quantity of cement; silica fume; water reducing admixtures (superplasticizers) and a low water content with a water-to-cement ratio of 0.16 [18].

4.3 Test setup and loading

In the test setup illustrated in Fig. 5, the beams' end spans were equipped with external vertical prestressing that prevented a shear failure in these regions.

Thus, the flexure-shear cracks and the beam collapse were confined to the center span.

The beams were placed on two intermediate supports, one a pin and the other a roller support placed on two massive concrete blocks. At each end, a cross beam was placed over the specimen and was anchored to the strong floor by means of a pair threaded steel rods on its either end. On the cross beams, the anchorage of each rod was equipped with a load cell.

The tests were displacement controlled. The displacement was applied in two consecutive stages:

In the first stage, the two cantilever ends of the beams were lowered by means of tightening the rods at each end; thus, a constant negative moment was applied along the center span (Fig. 6a). The imposed support rotation reduced the shear strength of the RC element in the central span over each support. The rods were tightened until an average force $Q_0/2$ of approximately 38.0 kN, in each rod. This stage of displacement was carried out over several steps, during which the deflections along the beam and the forces in the rods were measured to check for symmetry. After reaching the targeted moment, the vertical displacement at the cantilever ends was locked. At the end of this stage, the average measured deflection of the two ends of beams C1 and C2 were 5.9 and 4.6 mm, respectively. Thus, the mid spans of the beams were respectively lifted to 1.55 and 1.64 mm.

In the second stage, a downward displacement was applied at the mid span by means of a hydraulic jack attached to an isolated steel frame. The tests were carried out up to the maximum jack displacement mid-span. In this process, two flexure-shear cracks developed successively in the main span next to each support. The concrete fracture caused a local loss of the member resistance.

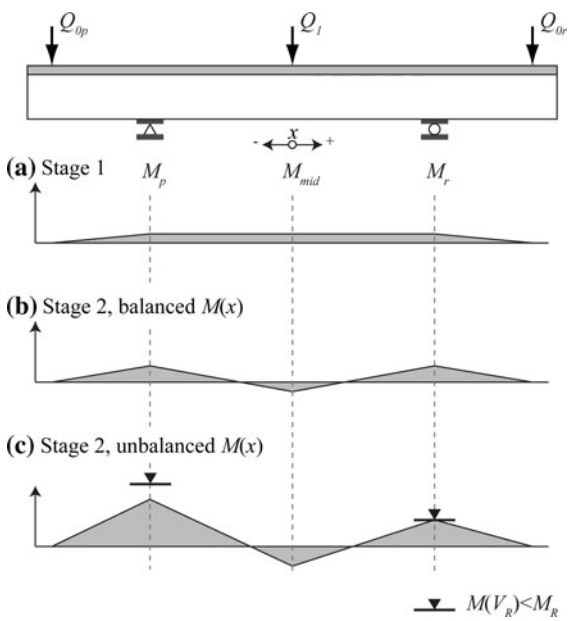

Fig. 6 Moment distribution during the test

The first hinging develops close to the roller support, where the stirrup spacing is the highest. As the displacement is increased, a second hinging in the beam also develops over the pin. Prior to the first hinging resistance, the force distribution along the beam was symmetric (Fig. 6b). After the first hinging resistance, the moment over the roller was limited to the residual resistance of the RU–RC beam. With the beam at the pin and the mid span providing extra resistance, the moment distribution diagram became unbalanced (Fig. 6c). The test continued into the post-hinging regime up to the maximum displacement, following which the beams were unloaded.

The test on beam C1 included two loading cycles, while beam C2 was loaded once. The test setup of beam C1 had to be adjusted between the two cycles. Except for a number of hairline flexural cracks the beam was undamaged after the first cycle. Indeed the force–displacement curves of the two cycles show a linear response. Each loading cycle was carried out during 1 day. In between the two cycles the beam was fully unloaded and left on the support. In the period between the two cycles, the downward mid-span deflection of the beam increased from 0.5 to 0.9 mm. This change is attributed to the relaxation of the member.

4.4 Instrumentation

A series of load cells were used to measure the force in the jack, the reaction force at the roller, and the force in the rods while applying the displacement in the first stage and throughout the test. Thus, it was possible to calculate the moment and shear force distribution in the system. The jack displacement relative to the frame was measured by means of a linearly variable displacement transformer (LVDT). A series of LVDTs measured the beam's deflection along the spans and its

vertical and horizontal displacements at the supports, with respect to the floor. Furthermore, two pairs of diagonal LVDTs on the RC element of the continuous beams were installed to measure the opening of flexure–shear cracks. A series of Ω-shaped extensometers with a base length of 100 mm measured the UHPFRC deformations along the top and bottom fibers. Across the UHPFRC and concrete interface, a series of mountable gauges measured the vertical deformation of the ICD zone due to cracks in concrete. All of the aforementioned instruments, including the load cells, took automatic measurements.

At chosen displacement levels, a demountable displacement transducer was used to measure the relative displacements and crack widths between a series of targets on three longitudinal lines on the surface of the UHPFRC element at different heights, a grid of equilateral triangles on the side of the RC element and obtuse isosceles triangles across the interface between UHPFRC and concrete.

All instruments were zeroed only once at the beginning of the test just before tightening of the rods at each end of the beam. During the test on beam C1, the automatic instruments continuously took measurements. No significant change was recorded over night between the two loading cycles.

5 Results and discussion

5.1 Member response

The beams have a similar structural response. The maximum resistance corresponds to the formation of a second support hinge due to the complete development of a flexure–shear collapse mechanism close to the pin. The second support hinge forms at an average resistance and rotation capacity that were 1.3 and 4.5 times the respective values at the first support hinge. This result clearly illustrates the ability of the beams to redistribute the stresses.

Both beams failed in the intermediate span, first at the roller (where the ratio of shear reinforcement in the RC element is lowest) and at the pin support. The response of the beams in Fig. 7 and their crack pattern in Fig. 8 show their similar behavior. The maximum resistance and the mid-span deflection for beam C1 were 245.1 kN and 7.4 mm and for beam C2 were 240.3 kN and 8.2 mm, respectively.

Figure 7 shows the response of each beam throughout the test. The plots for beam C1 include the first loading cycle, whose peak corresponds to a jack force of 160 kN, and the unloading due to the temporarily loss of the jack pressure, during which the jack force decreased from 215 to 136 kN.

Figure 7a, b show the plots of jack force versus the mid-span displacement (Δ_{mid}) of the beams. These plots indicate selected steps during the test. The step numbers with the prime symbol indicate sudden drops in the resistance. These drops correspond to the formation of the flexure–shear mechanism in the beam at each support. To illustrate the influence of the local flexure-shear cracks at each support, Fig. 7c, d show the measured reaction force at the roller (R_r) and the calculated reaction force at the pin (R_p).

Table 3 summarizes the results. At selected Δ_{mid} for each beam, the table lists the measured forces in the jack (Q_1), the cross beam close to the pin support (Q_{0p}) and the cross beam close to the roller support (Q_{0r}) as well as the support reactions (i.e., R_r and R_p). The table also provides the calculated shear forces acting in the center span from the mid span to the pin (V_p) and to the roller (V_r), followed by the ratio between the two. Finally, the table provides the moments over the pin (M_p), at the mid span (M_{mid}) and over the roller (M_r).

The internal shear forces and moments are based on an iterative calculation using the moment distributions and the three measured downward forces acting on the beams. Based on this calculation, the average error between the calculated and measured values of the reaction force at the roller is 9 %.

Despite the higher steel reinforcement ratio in the R-UHPFRC element of beam C2, the ultimate resistances of the beams in terms of the jack force are similar. Comparison has to be made using the reaction forces in Fig. 7 and the calculated shear forces in Table 3. The UHPFRC element of beam C1 and the R-UHPFRC element of beam C2 provide the required continuity for the moment redistribution following the shear failure. Indeed, a greater difference can be seen between the forces carried in the middle span of beam C2 than beam C1.

The resistance of the beams is directly linked to the tensile properties of the flexural reinforcement (both steel and UHPFRC) and the cracking behavior of the RC element. The latter is important in terms of the induced internal forces in the UHPFRC or the R-UHPFRC layer. The R-UHPFRC layer with the

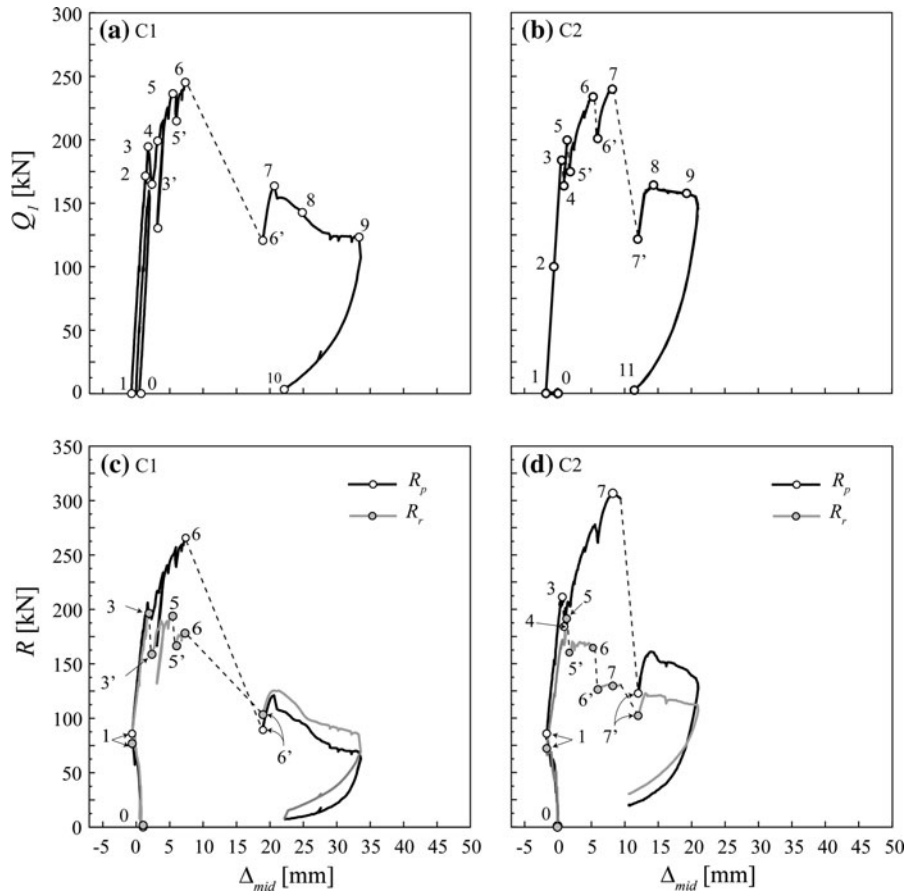

Fig. 7 Member response of Beams C1 and C2: **a**, **b** Jack force and **c**, **d** support reactions versus the mid-span displacement

steel reinforcing bars allows beam C2 to carry the higher shear force over the pin support. As shown in Fig. 8, beam C2 has a flat flexure–shear cracks on either side of the jack, while beam C1 has a flat crack over the pin but an almost vertical crack over the roller. At the mouth of the flexure-shear cracks the reinforcing overlay is subjected to combined tension and bending, a more severe condition than pure tension over a vertical crack.

5.2 Cracking behavior

The crack patterns in Fig. 8 give indications of the state of stress and strains in each element and the shear stress transfer between the two. The crack widths in the figure are the manual measurements taken at each step. These measurements were verified visually with a crack measurement ruler. At Step 1 in beam C1, the flexural crack from the bottom concrete face close to the mid span was from the first loading cycle.

The initial negative moment following the first stage of displacement caused a series of well-spaced, hairline, flexural cracks in the RC element that initiated at the interface between the two elements. Between the mid span and the pin, the crack position coincided with the location of the stirrups at 250 mm spacing. In the other half of the central span, the average crack spacing was approximately a third of the stirrup spacing of 400 mm.

Note that with the application of the negative moment in beam C1 up to Step 1, some localized debonding crack in the near-interface concrete zone close to the jack appeared (see Fig. 8a, Step 1). This crack initiated at the mouth of a flexural crack from the first loading cycle. The length of this crack was limited to the subsequent flexural crack.

With the introduction of positive moment at the mid span and the increasing mid-span deflection, both members began to crack at the mid-span; nevertheless, the crack width below the jack remained less than

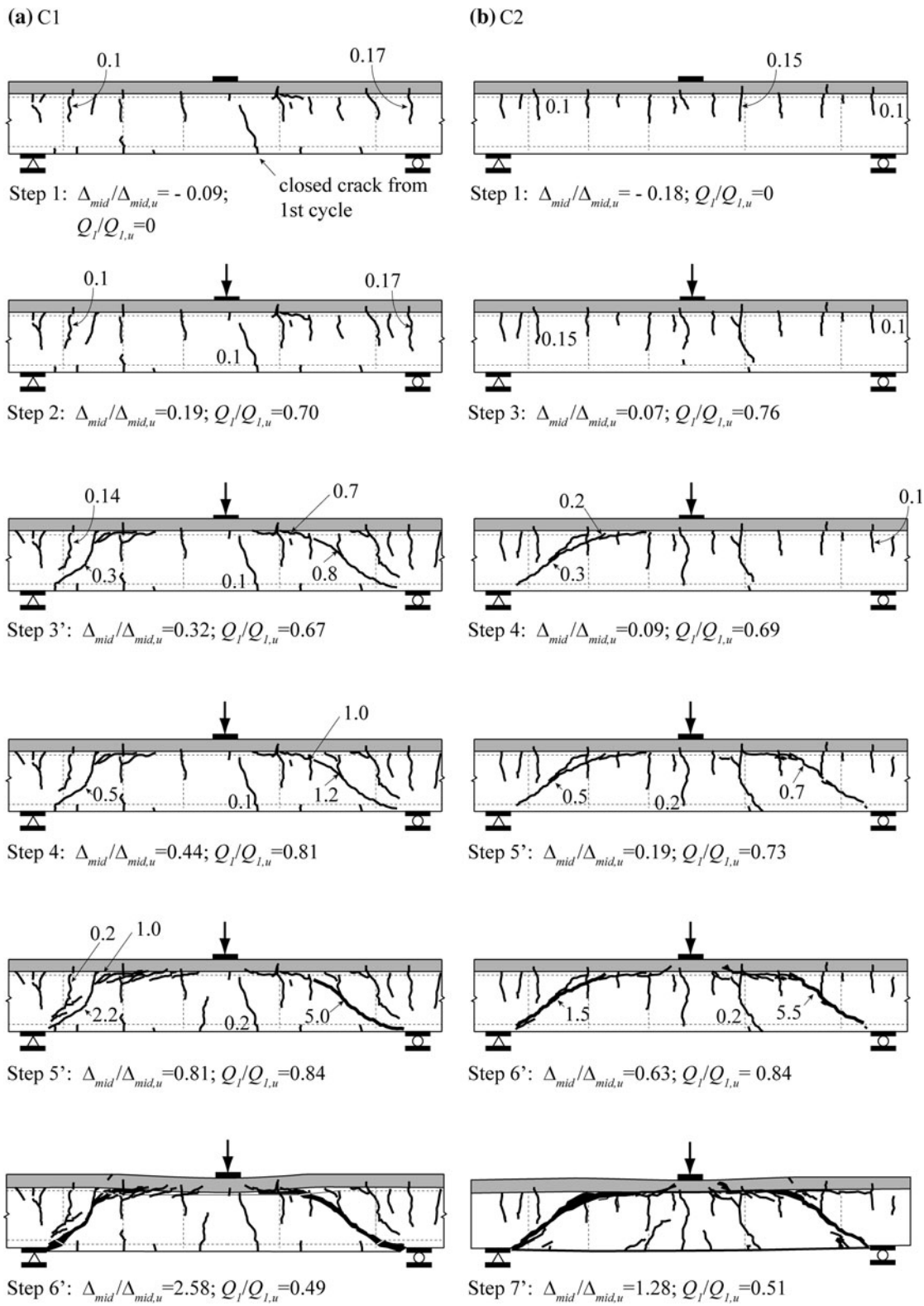

Fig. 8 Development of crack pattern of continuous beams

Table 3 Measured and calculated forces and moments

Beam	Step	Δ_{mid} (mm)	Q_1 (kN)	Q_{0p} (kN)	Q_{0r} (kN)	R_r (kN)	R_p (kN)	V_p (kN)	V_r (kN)	$-V_p/V_r$	M_p (kNm)	M_{mid} (kNm)	M_r (kNm)
C1	3	1.8	194.5	104.4	102.6	−182.6	−218.9	−97.9	96.6	1.01	−57.4	20.9	−56.4
	5	5.5	236.3	117.0	89.2	−181.0	−261.5	−127.7	108.6	1.18	−64.4	37.8	−49.1
	6	7.4	245.1	121.9	75.6	−166.0	−276.6	−138.5	106.6	1.30	−67.0	43.7	−41.6
	6′	19.0	120.6	32.1	40.5	−95.9	−97.3	−57.4	63.2	0.91	−17.7	28.3	−22.3
	9	33.3	123.3	11.4	19.2	−84.9	−69.0	−59.0	64.3	0.92	−6.3	40.9	−10.6
C2	5	1.5	200.1	94.5	104.6	−192.4	−206.8	−96.6	103.5	0.93	−52.0	25.3	−57.5
	6	5.2	234.5	126.5	79.4	−164.6	−275.8	−133.4	101.1	1.32	−69.6	37.2	−43.7
	7	9.4	240.3	142.5	53.4	−129.6	−306.6	−150.8	89.5	1.67	−78.4	42.2	−29.4
	7′	12.0	122.4	52.6	50.0	−102.2	−122.8	−62.1	60.3	1.03	−28.9	20.7	−27.5
	9	19.3	158.2	53.6	45.9	−113.5	−144.2	−81.8	76.4	1.07	−29.5	35.9	25.2

Note The internal shear forces and moments are calculated using the moment distribution method and only the three measured downward forces

0.1 mm. Up to their maximum resistance, both beams remained elastic at the mid span.

At a force level of 75–85 % of the maximum force, flexure–shear cracks in the center span close to the support appeared. With the appearance of these diagonal cracks, smeared cracks in the ICD zone were observed. The flexure-shear cracks developed towards the supports close to the level of the bottom longitudinal reinforcement. After the appearance of the flexure–shear cracks, the rotation of the RC element was concentrated about their crack tips, whereas the R-UHPFRC element close to the support rotated about the location of the mouth of the flexure–shear cracks in the RC element.

The cracks close to the support of beam C1 appeared almost instantaneously, following which the beam resistance was dropped by 20 %. The cracks next to the pin and the roller were at an average angle of 40° and 30° from the horizontal axis, respectively. In contrast, the flexure–shear cracks in beam C2 appeared one after the other. The drops in the force corresponding to the appearance of each crack were between 15 and 17 %. The cracks next to the pin and the roller were respectively at an angle of 33° and 35° from the horizontal axis. The flexure-shear cracks were positioned so that there were no stirrups crossing the first half of the crack. With increasing displacements, these cracks formed the collapse plane of the beam.

Close to 95 % of the maximum force, the resistance dropped by 10–15 % and the crack widths suddenly increased. The opening of the flexure–shear crack caused the ICD zone to develop further towards the jack at the mid span, where the cracks kinked into the R-UHPFRC layer towards the steel loading plate between the jack and the beam. At peak, the failure occurred with the full formation of the second flexure–shear collapse mechanism.

The photo in Fig. 9 clearly illustrates how the continuous member changes into a system of three concrete rigid bodies divided by the collapse cracks. The rigid bodies were bridged by the steel rebars in the concrete and R-UHPFRC element.

5.3 Member deformation

During the tests, the appearance of flexure-shear cracks of the RC element over the roller support caused small sudden drops of resistance. The latter was due to the crushing of concrete at the tip of the collapse crack [17]. Following the local drop of resistance, the stresses redistributed and were directed to the stiffer sections of the beam. With the increasing applied actuator displacement, the beams showed increasing force up to the maximum resistance (i.e., peak at Step 6 for beam C1 and Step 7 for beam C2, respectively).

The difference between the maximum jack force ($Q_{1,u}$) acting at the mid span of the beams is only 2 %, while the mid-span deflection at this force ($\Delta_{mid,u}$) of beam C2 is 11 % higher than the displacement of the other beam. The higher rotation capacity is attributed

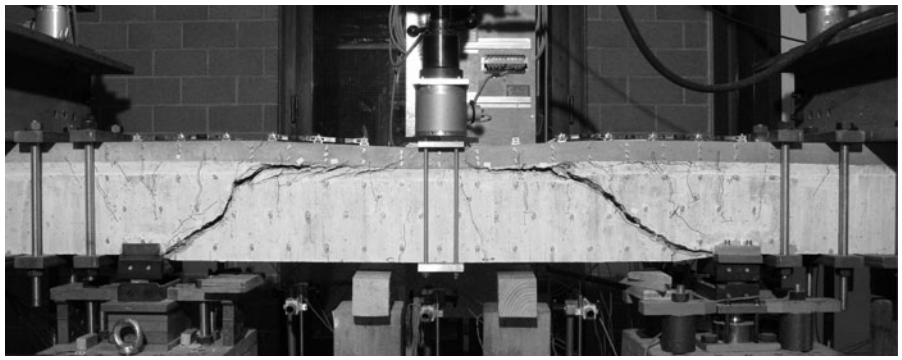

Fig. 9 Crack pattern of beam C1 in the post-hinging domain close to the end of the test

to the longitudinal steel reinforcement in the R-UHPFRC element of beam C2.

The plots of the reaction forces versus the mid-span displacement in Fig. 7 reveal the loss of the beams' resistance over the roller support ahead of the pin support. In Fig. 7c, the hinging in beam C1 occurs between Steps 3 and 3′. In Fig. 7d, the hinging in beam C2 at the roller occurs in two stages from Steps 5 to 5′ and 6 to 6′. As illustrated in Fig. 8a (Step 3′) and Fig. 8b (Steps 5′ and 6′), the losses in resistance were due to two mechanisms: First, the development of the flexure-shear cracks, reducing the contribution of concrete; Second, the formation of the ICD zone between the elements that extends the length of the R-UHPFRC carrying the shear stresses in double curvature [16].

The cracking behaviors of the beams up to the maximum resistance were different in each half of the central span; thus, the beams' deformed shapes were asymmetrical about the mid span (Fig. 10). In beam C1, the first support hinge forms at Step 3. In contrast, the drop in beam C2 at Step 3 was due to the appearance of the first flexure–shear crack in the beam close to the pin (Fig. 8); beam C2's first hinging occurred at Step 5. After the first hinging, the stresses redistributed and more force was transferred to the pin support. Nevertheless, the beams were able to continuously carry part of the stresses over the roller support. In the pre-peak regime, the reduction of the beam resistance at the roller caused Q_1 to drop between 10 and 20 %. In terms of the shear forces in the central span, the shear forces in beams C1 and C2 at the pin were respectively up to 1.30–1.67 times higher than the shear forces at the roller. This is due to the significant difference between the beam stiffness over each support: Over the pin, the composite beam is still monolithic while over the roller the beam has changed into a two-layer member. The stiffness of each

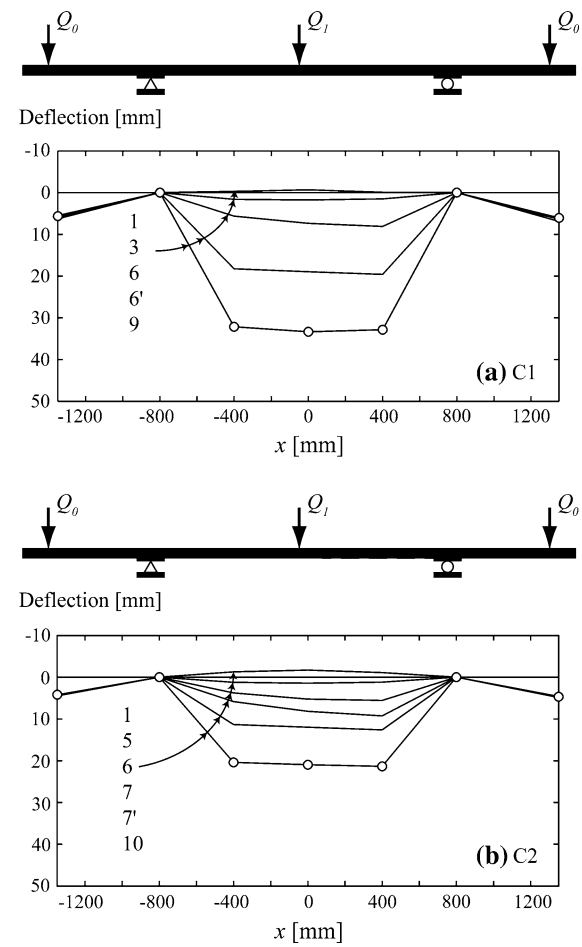

Fig. 10 Deformed shapes of continuous beams

segment is similar to that of the cantilever beams in Fig. 1. The high member resistance makes it possible for the pin to provide the necessary resistance.

At peak, the beams failed due the complete development of the second flexure-shear crack next to the pin support. The drop in the beams' resistance was approximately 50 % of their respective $Q_{1,u}$. Following the failure, the mid-span displacements of beams C1 and C2 respectively increased by 2.6 and 1.5 times $\Delta_{\text{mid},u}$. With the collapse of the beams, the deformed shapes became symmetrical (e.g., compare the deformed shape of Steps 7 and 7′ in Fig. 10b).

In the post-hinging domain, the tests on beams C1 and C2 were carried out up to a maximum mid-span deflection of 34 and 21 mm, respectively. The deformations in the R-UHPFRC element eventually concentrated above the mouth of the flexure–shear cracks in the RC element, where the R-UHPFRC element was subjected to combined tension and bending [17]. The reduction in the resistance of the beam in the post-hinging domain is due to the softening of the UHPFRC. The average post-hinging resistances of beams C1 and C2 were 129.0 kN and 152.4 kN (53 and 63 % of the maximum jack force), respectively.

6 Conclusions

This paper presents the experimental program carried out to study the structural response of continuous RU–RC beams with a lower flexure-shear resistance in the intermediate span over one of the two supports. The local formation of a flexure-shear collapse mechanism in the continuous RU–RC beam over a support is referred to as hinging. The following conclusions were reached:

1. R-UHPFRC elements increase member redundancy by carrying the redistributed stresses following the hinging resistance of the beams.
2. Over the supports, the capacity of the beam to carry the redistributed stresses strongly depends on the post-hinging resistance that is the sum of the contributions of the R-UHPFRC element (in combined bending and tension), the longitudinal steel rebars in the RC element (i.e., the tensile membrane action of the tensile rebars and dowel action of the compressive rebars over the support), and the stirrups.
3. In the post-hinging regime, the bending resistance and the tensile membrane action of the R-UHPFRC element are the two principle mechanisms carrying the force, in a way much similar to a stress-ribbon structure.
4. Under positive moments at the center of the continuous beams, the UHPFRC elements with a high compressive strength acts as a strong flange. At mid span, the neutral axis is located within the thickness of the R-UHPFRC element. This increases both in member resistance and rotation capacity. Additionally, the inclined compressive stresses in the layer contribute to the shear resistance. The behavior of beams with the R-UHPFRC layer in compression has to be studied in further detail.
5. Acting as a stress ribbon in combined tension and bending, the R-UHPFRC element provides member continuity and gives the structural system the capability to gradually loose its load carrying capacity and to have a graceful degradation until the ultimate resistance.

References

1. Alaee FJ, Karihaloo BL (2003) Retrofitting of reinforced concrete beams with CARDIFRC. J Compos Constr 7(3): 174–186
2. Brühwiler E, Denarié E (2008) Rehabilitation of concrete structures using ultra-high performance fibre reinforced concrete. In: Ultra high performance concrete (UHPC), Kassel, The Second International Symposium on Ultra High Performance Concrete
3. Bachmann H (1967) Zur plastizitätstheoretischen Berechnung statisch unbestimmter Stahlbetonbalken. Doctoral Thesis, ETH Zürich
4. Dilger W (1966) Veränderlichkeit der Biege- und Schubsteifigkeit bei Stahlbetontragwerken und ihr Einfluss auf Schnittkraftverteilung und Traglast bei statisch unbestimmter Lagerung. Wilhelm Ernst & Sohn, Berlin
5. Habel K (2004) Structural behaviour of elements combining ultra-high performance fibre reinforced concretes (UHPFRC) and reinforced concrete. Dissertation, EPFL
6. Habel K, Denarié E, Bruhwiler E (2006) Structural response of elements combining ultrahigh-performance fiber-reinforced concretes and reinforced concrete. J Struct Eng 132(11):1793–1800
7. Kani GNJ (1966) Basic Facts Concerning Shear Failure. ACI J Proc 63(6):675–692
8. Kim YY, Fischer G, Li VC (2004) Performance of Bridge Deck Link Slabs Designed with Ductile ECC. ACI Struct J 101(6):792–801
9. Marti P, Pfyl T, Sigrist V, Ulaga T (1999) Harmonized Test Procedures for Steel Fiber-Reinforced Concrete. ACI Struct J 96(6):676–686

10. Y (2010) Post-punching behavior of reinforced concrete slabs. Dissertation, EPFL
11. Muttoni A, Schwartz J (1991) Behaviour of Beams and Punching in Slabs without Shear Reinforcement. Proc IABSE Colloquium 62:703–708
12. Fernández Ruiz M, Muttoni A, Kunz J (2010) Strengthening of flat slabs against punching shear using post-installed shear reinforcement. ACI Struct J 107(4):434–442
13. Muttoni A (2008) Punching Shear Strength of Reinforced Concrete Slabs without Transverse Reinforcement. ACI Struct J 105(4):440–450
14. Naaman AE, Reinhardt HW (2006) Proposed classification of HPFRC composites based on their tensile response. Mater Struct 39:547–555
15. Noshiravani T (2011) Fracture test of R-UHPFRC–RC composite beams subjected to combined bending and shear. Test Report. MCS, EPFL
16. Noshiravani T (2012) Structural response of R-UHPFRC–RC composite members subjected to combined bending and shear. Dissertation, EPFL
17. Noshiravani T, Brühwiler E (2013) Experimental investigation on R-UHPFRC–RC composite beams subjected to combined bending and shear. ACI Struct J, 110 (2)
18. Oesterlee C (2010) Structural response of reinforced UHPFRC and RC composite members. Dissertation, EPFL
19. Schumacher P (2006) Rotation capacity of self-compacting steel fiber reinforced concrete. Dissertation, Delft University of Technology
20. Stang H, Li VC (2004) Classification of Fibre Reinforced Cementitious Materials for Structural Applications. 6th RILEM Symposium on fibre reinforced concrete (FRC)—BEFIB 2004, Varenna, Italy: 197–218
21. Teng JG, Chen JF, Smith ST, Lam L (2003) Behaviour and strength of FRP-strenghtened RC structures: a state-of-the-art review. Proceedings of the Institution of Civil Engineers Structures & Buildings, 156, Institution of Civil Engineers, London, Great Britain: 51–62
22. Wuest J (2007) Comportement structural des bétons de fibres ultra performants en traction dans des éléments composés. Dissertation, EPFL